MULTI-BAND NEGATIVE REFRACTIVE INDEX IN FERRITE-BASED METAMATERIALS

Ke Bi[1], Ji Zhou[1, *], Xiaoming Liu[1], Chuwen Lan[1], and Hongjie Zhao[2]

[1]State Key Laboratory of New Ceramics and Fine Processing, School of Materials Science and Engineering, Tsinghua University, Beijing 100084, P. R. China

[2]Aerospace Research Institute of Special Materials and Processing Technology, Beijing 100074, P. R. China

Abstract—A multi-band ferrite-based metamaterial has been investigated by experiments and simulations. The negative permeability is realized around the ferromagnetic resonance (FMR) frequency which can be influenced by the saturation magnetization $4\pi M_s$ of the ferrites. Due to having multiple negative permeability frequency regions around the multiple FMR frequencies, the metamaterials consisting of metallic wires and ferrite rods with various $4\pi M_s$ possess several passbands in the transmission spectra. The microwave transmission properties of the ferrite-based metamaterials can be not only tuned by the applied magnetic field, but also adjusted by the $4\pi M_s$ of the ferrite rods. A good agreement between experimental and simulated results is demonstrated, which confirms that such a ferrite-based metamaterial possesses a tunable multi-band behavior. This approach opens a new way for designing multi-band metamaterials.

1. INTRODUCTION

Electromagnetic metamaterial is a composite in which subwavelength features, rather than the constituent materials, control the macroscopic electromagnetic properties. Negative refractive index (NRI) metamaterials with simultaneously negative permittivity and negative permeability are currently the focus of a great deal of interest due to their unique electromagnetic properties such as the reversals of

both Doppler shift and Cherenkov radiation, enhancement of evanescent wave, and subwavelength resolution imaging, etc. [1–9]. Most of the reports demonstrated the NRI metamaterials realized by periodic artificial metallic structures [10–15]. For instance, using periodic split-ring resonators (SRRs) to provide effective negative permeability and using periodic continuous wires to produce effective negative permittivity [16, 17]. By adjusting the structural sizes of the metallic resonators to achieve the effective negative permeability, metamaterials can show the controllable electromagnetic properties. Recently, research has focused on the ability to design broadband or multi-band metamaterials for multi-frequency applications [18, 19]. The current multi-band metamaterials are fabricated by using two or more different artificial metallic resonators [20–24]. However, due to the immutable structures of the unit cell, those metamaterials only have a narrow band and can not be tuned. Moreover, the dimension of the periodic composite structure should be small enough compared to the wavelength, which creates challenges in the fabrication [25].

It is well known that gyromagnetic materials can exhibit a negative permeability at the ferromagnetic resonance (FMR) frequency range [26, 27]. Hence, the possibility of producing NRI metamaterials with gyromagnetic materials has been widely discussed in theory and many structures have been proposed [28–30]. As the most typical gyromagnetic materials, ferrites were used to substitute for SRRs to provide a more dynamically tunable negative permeability [31, 32]. Under an applied bias magnetic field, ferrite-based metamaterials show a tunable NRI characteristic in a broad frequency band [33, 34]. Much effort has been put into the fabrication and investigation of dual-band NRI metamaterials composed of ferrites and metallic resonators [35]. But the structure is too complex and only one band which provided by ferrites can be tuned.

Here, we demonstrate a new strategy for obtaining the extremely broad band or multi-band metamaterials through ferrite-based structures with various saturation magnetizations. To prove the multi-band behavior, the microwave transmission properties of ferrite-based metamaterials tuned by the saturation magnetization of the ferrite were investigated by experiments and simulations.

2. EXPERIMENTAL PROCEDURE

The commercial yttrium iron garnet (YIG) rods were sliced with dimensions of $l \times w \times h \, \text{mm}^3$, where $l = 1 \, \text{mm}$, $w = 0.5 \, \text{mm}$, $h = 10 \, \text{mm}$, respectively. The linewidth ΔH and relative permittivity ε_r of the YIG rods are $10 \, \text{Oe}$ and 14.5. The saturation magnetization $4\pi M_s$

is 1200 Gs, 1400 Gs, 1600 Gs, and 1950 Gs, respectively. Firstly, the YIG rods with $4\pi M_s$ of 1200 Gs and 1400 Gs were pasted together while the YIG rods with $4\pi M_s$ of 1600 Gs and 1950 Gs were pasted together to obtain a kind of YIG rod with two different $4\pi M_s$ and a size of $1 \times 1 \times 10 \, \text{mm}^3$, as shown in Fig. 1(a). Secondly, by using a shadow mask/etching technique, we prepared 0.3 mm thick FR-4 dielectric substrates ($\varepsilon_r = 4.4$ and $\tan \delta = 0.014$) with copper wires spacing of 4 mm on one side. The size of the copper wires is $0.5 \times 0.03 \times 10 \, \text{mm}^3$. The other 0.3 mm thick FR-4 dielectric substrates without copper wires were pasted on the side of dielectric substrates with copper wires, which made two sides of the copper wires covered by the dielectric substrates. Thirdly, the YIG rods with $4\pi M_s$ of 1200 Gs and 1400 Gs were pasted back-to-back with copper wires on one side of the substrate/wire/substrate structure while the YIG rods with $4\pi M_s$ of 1600 Gs and 1950 Gs were pasted back-to-back with copper wires on the other side of the substrate/wire/substrate structure. The four ferrite rods with various saturation magnetization $4\pi M_s$ and one copper wire formed a four rods-one wire unit, which is shown as an inset in Fig. 1(a). The multi-band NRI ferrite-based metamaterials were obtained by assembled the four rods-one wire units into an array, as shown in Fig. 1(a). The distance d between the rods is 3 mm. For comparison, the single-band NRI ferrite-based metamaterials were also prepared by assembled the rod-wire units into an array. The structure of the single-band NRI ferrite-based metamaterials is same as that
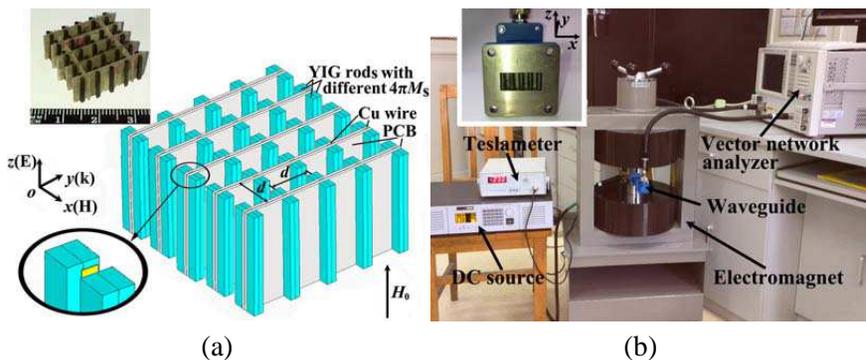

(a)   (b)

Figure 1. (a) Schematic diagram and photograph of the multi-band NRI ferrite-based metamaterials. (b) Photograph of the measurement system composed of a vector network analyzer and an electromagnet. The inset shows the photograph of the sample in the cross section of the waveguide.

in [33].

The microwave properties of the ferrite-based metamaterials were measured by an HP 8720ES network analyzer. The measurement system composed of a vector network analyzer and an electromagnet is shown in Fig. 1(b). The multi-band or single-band NRI ferrite-based metamaterials were placed in an X-band rectangular waveguide WR90 ($22.86 \times 10.16 \, \text{mm}^2$) to measure the scattering parameters. The photograph of the metamaterials in the cross section of the waveguide is shown as an inset in Fig. 1(b). The waveguide was put in the middle of two magnets. By adjusted by input current, a bias magnetic field was generated around the samples along the z direction. The microwave with TE$_{10}$ mode propagates along y direction with the electric field along the z direction and the magnetic field along the x direction. In addition, the microwave properties of unit cells of multi-band ferrite-based metamaterials were simulated by using CST Microwave Studio, a Maxwell's equations solver. The geometry, dimensions and material parameters for the simulation are chosen to be consistent with the experimental ones.

3. EXPERIMENTAL RESULTS AND DISCUSSION

It is well known that the negative permeability of the ferrite can be obtained when the FMR takes place. The effective permeability of the ferrite can be expressed by [33]

$$\mu_{eff}(\omega) = 1 - \frac{F\omega_{mp}^2}{\omega^2 - \omega_{mp}^2 - i\Gamma(\omega)\omega} \tag{1}$$

with

$$\Gamma(\omega) = \left(\frac{\omega^2}{\omega_r + \omega_m} + \omega_r + \omega_m\right)\alpha \tag{2}$$

$$\omega_{mp} = \sqrt{\omega_r(\omega_r + \omega_m)} \tag{3}$$

$$\omega_m = 4\pi M_s \gamma \tag{4}$$

$$\omega_r = \gamma\sqrt{[H_0 + H_a + (N_x - N_z)\, 4\pi M_s]\, [H_0 + H_a + (N_y - N_z)\, 4\pi M_s]} \tag{5}$$

where α is damping coefficient of ferromagnetic precession, γ the gyromagnetic ratio, $F = \omega_m/\omega_r$, ω_m the characteristic frequency of the ferrite, ω_r the FMR frequency of the ferrite, M_s the saturation magnetization, H_0 is the applied magnetic field, H_a the magnetocrystalline anisotropy field, and N_x, N_y, and N_z are the demagnetization factor for x, y, and z directions, respectively. From Eqs. (1)–(5), it can be predicted that the saturation magnetization

$4\pi M_s$ affects both the FMR frequency ω_r and the characteristic frequency ω_m, and further influence the effective permeability of the ferrite. Based on Eq. (5), the ω_r increases as the $4\pi M_s$ increases, which can lead to the negative $\mathrm{Re}(\mu_{eff})$ frequency region shifting to the higher frequency.

The single-band NRI ferrite-based metamaterial is composed of copper wires and YIG rods with $4\pi M_s = 1950\,\mathrm{Gs}$. Fig. 2(a) shows the measured transmission spectra for rods-only, wires-only and the single-band NRI ferrite-based metamaterial, respectively. One observes that there is a band gap and stop band in the transmission curves for YIG rods alone and wires alone, which are induced by the negative permeability of the ferrite around the FMR frequency and negative permittivity of the wires array within a wide region below the electric plasma frequency, respectively. Besides, a passband, which emerges just in the region where both permittivity and permeability are negative, was observed for the ferrite-based metamaterial consisting of copper wires and YIG rods with $4\pi M_s = 1950\,\mathrm{Gs}$. The measured transmission spectra for the single-band NRI ferrite-based metamaterials with a series of $4\pi M_s$ were shown in Fig. 2(b). It can be seen that the passband measured with different $4\pi M_s$ reveals a tunable property. The passband frequency increases from 8.2 to 9.7 GHz as $4\pi M_s$ increases from 1200 Gs to 1950 Gs, which shows that the transmission property is influenced by the saturation magnetization $4\pi M_s$ related to the FMR frequency ω_r. This characteristic can be used to prepare the multi-band metamaterials consisting of metallic wires
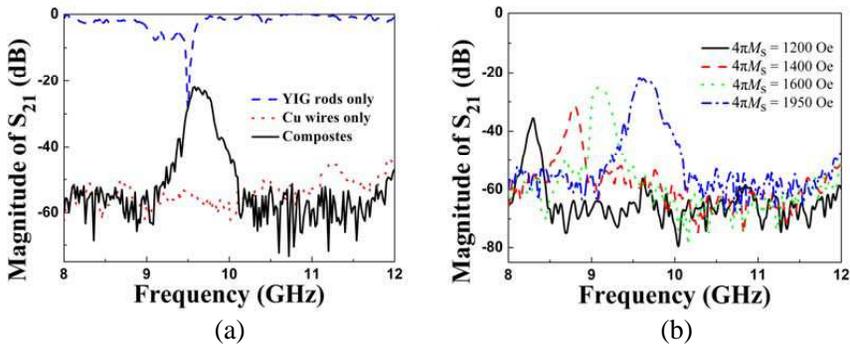

Figure 2. (a) Measured transmission spectra for rods-only, wires-only and the single-band NRI ferrite-based metamaterial with $4\pi M_s = 1950\,\mathrm{Gs}$ at $H_0 = 2300\,\mathrm{Oe}$. (b) Measured transmission spectra for the single-band NRI ferrite-based metamaterials with a series of $4\pi M_s$ at $H_0 = 2300\,\mathrm{Oe}$.

and ferrite rods with various $4\pi M_s$.

The multi-band NRI ferrite-based metamaterials are composed of four rods-one wire units. The saturation magnetizations $4\pi M_s$ of the four ferrite rods are 1200 Gs, 1400 Gs, 1600 Gs, and 1950 Gs, respectively. Fig. 3 shows the measured transmission spectra for four rods-only, wires-only and the multi-band NRI ferrite-based metamaterials with various $4\pi M_s$ at $H_0 = 2300$ Oe. There are four band gaps in the transmission curve for four YIG rods alone, which is induced by the negative permeability around the four FMR frequency regions. Because the paasband controlled by the YIG rod with $4\pi M_s = 1600$ Gs connects with that controlled by the YIG rod with $4\pi M_s = 1950$ Gs, one broad passband and two narrow passbands are observed for the multi-band NRI ferrite-based metamaterials consisting of the four rods-one wire units, which is different from the transmission spectra observed for ferrite-based metamaterials consisting of rod-wire units. By adjusting the combination of the YIG rods with different $4\pi M_s$, we can not only obtain various multi-band metamaterials such as dual-band, three-band, and four-band metamaterials, but also acquire the multi-band metamaterials with tunable passband frequency region.
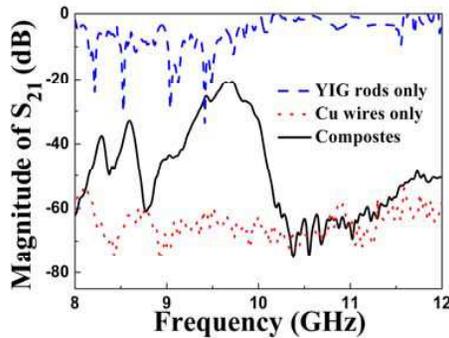

Figure 3. Measured transmission spectra for four rods-only, wires-only and the multi-band NRI ferrite-based metamaterials with different $4\pi M_s$ at $H_0 = 2300$ Oe.

4. SIMULATIONS

Due to applying the electromagnet to provide the bias magnetic field, it is difficult to obtain precise measurements of the transmission and reflection by repeatedly assembling the waveguides and matching loads. Thus, instead of experimental data, the simulated scattering

parameters are used to retrieve the effective material parameters. The effective material parameters can be retrieved by the expressions [36]

$$\mu = nz \tag{6}$$
$$\varepsilon = n/z \tag{7}$$

with

$$n = \frac{1}{kd} \cos^{-1} \left[\frac{1}{2S_{21}} \left(1 - S_{11}^2 + S_{21}^2 \right) \right] \tag{8}$$

$$z = \sqrt{\frac{(1+S_{11})^2 - S_{21}^2}{(1-S_{11})^2 - S_{21}^2}} \tag{9}$$

where μ and ε are the effective permeability and permittivity, respectively. n is the refractive index, z the wave impedance of the sample, $k = \omega/c$, the wave number of the incident wave, d the thickness of a single unit cell of the structure, and S_{11} and S_{21} are the scattering parameters.

The unit cell of a ferrite rod alone with the dimension of $4 \times 4 \times 10 \, \text{mm}^3$ is shown in Fig. 4(a). The geometry, dimensions and material parameters used in the simulation are the same as the experimental ones. The magnetization direction of the ferrite rod is along the z-axis direction. The retrieved effective permeability μ_{eff} of the ferrite rod with a series of $4\pi M_s$ is shown in Fig. 4(b). The propagation of the electromagnetic wave is along the y axis, and the electric field and magnetic field are along z and x directions, respectively. The applied magnetic field was set at $H_0 = 2300 \, \text{Oe}$. Firstly, in all cases, there is one remarkable frequency dispersion in the range of 8–12 GHz and the
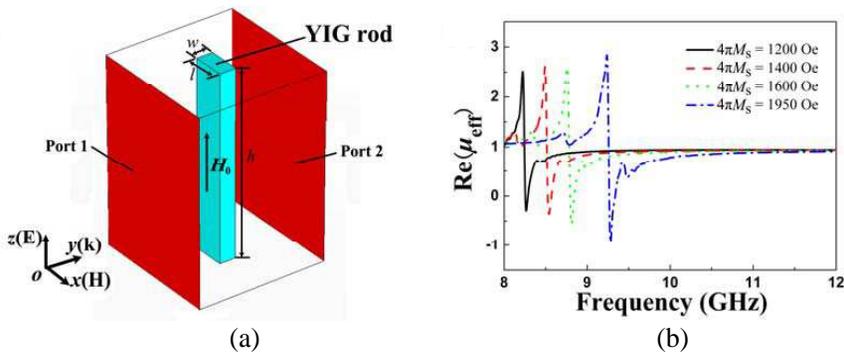

Figure 4. (a) Unit cell of a ferrite rod alone. (b) Real part of effective permeability retrieved from simulated scattering parameters with a series of $4\pi M_s$ at $H_0 = 2300 \, \text{Oe}$.

negative $\text{Re}(\mu_{eff})$ appears at the upper resonant frequencies. Secondly, one observes that the FMR frequency increases as the $4\pi M_s$ increases, which results in negative permeability frequency region shifting to the high frequency region. It can be seen that the behavior in simulated results is in good agreement with that observed in experimental ones.

The unit cell of four ferrite rods with different $4\pi M_s$ is shown in Fig. 5(a). The dimension of each ferrite rod is $1 \times 0.5 \times 10 \,\text{mm}^3$. The $4\pi M_s$ of the ferrite rods are $1200 \,\text{Gs}$, $1400 \,\text{Gs}$, $1600 \,\text{Gs}$, and $1950 \,\text{Gs}$, respectively. The retrieved effective permeability μ_{eff} of four ferrite rods with different $4\pi M_s$ at $H_0 = 2300 \,\text{Oe}$ is shown in Fig. 5(b). The four rods unit shows the four negative permeability frequency regions properties, which is different from that of the one rod unit shown in Fig. 4(b). Combined with Fig. 4(b), we can easily conclude that the first, second, third, and fourth negative permeability frequency regions are provided by the ferrite rod with $4\pi M_s = 1200 \,\text{Gs}$, $1400 \,\text{Gs}$, $1600 \,\text{Gs}$, and $1950 \,\text{Gs}$, respectively. It is obvious that each of four negative permeability frequency regions can be tuned by changing the $4\pi M_s$ of the ferrite rod.
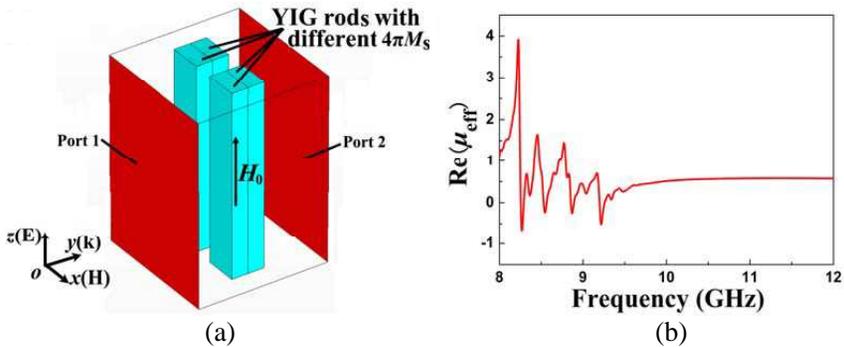

Figure 5. (a) Unit cell of four ferrite rods with different $4\pi M_s$. (b) Real part of effective permeability retrieved from simulated scattering parameters for the four ferrite rods with $4\pi M_s = 1200 \,\text{Gs}$, $1400 \,\text{Gs}$, $1600 \,\text{Gs}$, and $1950 \,\text{Gs}$, respectively.

A unit cell of four ferrite rods and one copper wire is shown in Fig. 6(a). The dimensions and material parameters of the ferrite rods and copper wire are the same as that described above. The real part of effective refractive index n_{eff} is retrieved from the simulated scattering parameters for the four rods-one wire unit, as shown in Fig. 6(b). It can be seen that there are four negative refractive indices appeared in the range of 8–12 GHz. The real part of the index $\text{Re}(n_{eff})$ is negative in the frequency range where the passband appears, indicating
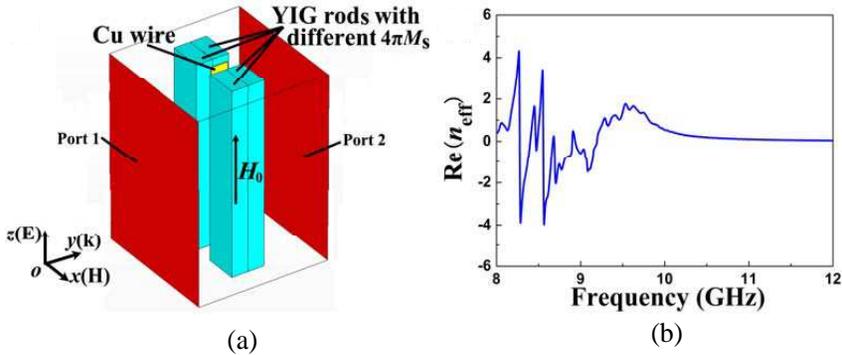
Figure 6. (a) Unit cell of four ferrite rods and one copper wire. (b) Retrieved real part of effective refractive index of the four rods-one wire unit with different $4\pi M_s$ at $H_0 = 2300\,\mathrm{Oe}$.

that the multi-band ferrite-based metamaterials should be the NRI metamaterials. The multi-band characteristic obtained in simulated results is in agreement with that observed in experimental ones.

Based on above analysis of experiments and simulations, one can design the extremely broadband or multi-band metamaterials by combining several ferrite rods with various saturation magnetizations into a unit cell. Each part of passband or each passband is controlled by a ferrite rod with a certain saturation magnetization and can be tuned by adjusting the saturation magnetization of each part of the unit cell.

5. CONCLUSION

The multi-band NRI ferrite-based metamaterials consisting of metallic wires and ferrite rods with various saturation magnetization $4\pi M_s$ have been prepared. The microwave transmission properties can be tuned not only by changing the applied magnetic field, but also by adjusting the $4\pi M_s$ of the ferrite rods. For the single-band NRI ferrite-based metamaterials consisting of rod-wire units, the passband frequency increases as $4\pi M_s$ of the ferrite rods increases. For the multi-band NRI ferrite-based metamaterials consisting of four ferrite rods-one copper wire units, there are two narrow passbands and one broad passband observed in the range of 8–12 GHz. One can design the extremely broad band or multi-band metamaterials by combining several ferrite rods with various saturation magnetizations into a unit cell. The results provide a new way to fabricate the tunable multi-band metamaterials cloaks, antennas and absorbers.

ACKNOWLEDGMENT

REFERENCES

1. Veselago, V. G., "The electrodynamics of substance simultaneously negative values of ε and μ," *Sov. Phys. Usp.*, Vol. 10, 509–514, 1968.

2. Pendry, J. B., "Negative refraction makes a perfect lens," *Phys. Rev. Lett.*, Vol. 85, 3966–3969, 2000.

3. Duan, Z., B.-I. Wu, S. Xi, H. Chen, and M. Chen, "Research progress in reversed Cherenkov radiation in double-negative metamaterials," *Progress In Electromagnetics Research*, Vol. 90, 75–87, 2009.

4. Gong, Y. and G. Wang, "Superficial tumor hyperthermia with flat left-handed metamaterial lens," *Progress In Electromagnetics Research*, Vol. 98, 389–405, 2009.

5. Cao, P., X. Zhang, L. Cheng, and Q. Meng, "Far field imaging research based on multilayer positive- and negative-refractive-index media under off-axis illumination," *Progress In Electromagnetics Research*, Vol. 98, 283–298, 2009.

6. Dong, W., L. Gao, and C.-W. Qiu, "Goos-Hänchen shift at the surface of chiral negative refractive media," *Progress In Electromagnetics Research*, Vol. 90, 255–268, 2009.

7. Seddon, N. and T. Bearpark, "Observation of the inverse Doppler effect," *Science*, Vol. 302, 1537–1540, 2003.

8. Danaeifar, M., M. Kamyab, A. Jafargholi, and M. Veysi, "Bandwidth enhancement of a class of cloaks incorporating metamaterials," *Progress In Electromagnetics Research Letters*, Vol. 28, 37–44, 2012.

9. Zhao, Y., F. Chen, H. Chen, N. Li, Q. Shen, and L. Zhang, "The microstructure design optimization of negative index metamaterials using genetic algorithm," *Progress In Electromagnetics Research Letters*, Vol. 22, 95–108, 2011.

10. Cheng, Y., Y. Nie, L. Wu, and R. Z. Gong, "Giant circular dichroism and negative refractive index of chiral metamaterial

based on split-ring resonators," *Progress In Electromagnetics Research*, Vol. 138, 421–432, 2013.

11. Xi, S., H. Chen, B.-I. Wu, and J. A. Kong, "Experimental confirmation of guidance properties using planar anisotropic left-handed metamaterial slabs based on S-ring resonators," *Progress In Electromagnetics Research*, Vol. 84, 279–287, 2008.

12. Chen, H., L. Ran, J. Huangfu, X. Zhang, K. Chen, T. M. Grzegorczyk, and J. A. Kong, "Negative refraction of a combined double S-shaped metamaterial," *Appl. Phys. Lett.*, Vol. 86, 151909, 2005.

13. Li, J., F.-Q. Yang, and J.-F. Dong, "Design and simulation of L-shaped chiral negative refractive index structure," *Progress In Electromagnetics Research*, Vol. 116, 395–408, 2011.

14. Wongkasem, N., A. Akyurtlu, and K. A. Marx, "Group theory based design of isotropic negative refractive index metamaterials," *Progress In Electromagnetics Research*, Vol. 63, 295–310, 2006.

15. Djeffal, Z. E., H. Talleb, D. Lautru, and V. Fouad-Hanna, "Negative refractive index behavior through magneto-electric coupling in split ring resonators," *Progress In Electromagnetics Research Letters*, Vol. 22, 155–163, 2011.

16. Martín, F., J. Bonache, F. Falcone, M. Sorolla, and R. Marqués, "Split ring resonator-based left-handed coplanar waveguide," *Appl. Phys. Lett.*, Vol. 83, 4652–4654, 2003.

17. Maslovski, S. I., S. A. Tretyakov, and P. A. Belov, "Wire media with negative effective permittivity: A quasi-static model," *Microwave Opt. Technol. Lett.*, Vol. 35, 47–51, 2002.

18. Zhong, J., Y. Huang, G. Wen, H. Sun, P. Wang, and O. Gordon, "Single-/dual-band metamaterial absorber based on cross-circular-loop resonator with shorted stubs," *Appl. Phys. A*, Vol. 108, 329–335, 2012.

19. Kang, L., Q. Zhao, H. Zhao, and J. Zhou, "Magnetic tuning of electrically resonant metamaterial with inclusion of ferrite," *Appl. Phys. Lett.*, Vol. 93, 171909, 2008.

20. Guo, W., L. He, B. Li, T. Teng, and X.-W. Sun, "A wideband and dual-resonant terahertz metamaterial using a modified SRR structure," *Progress In Electromagnetics Research*, Vol. 134, 289–299, 2013.

21. He, X.-J., Y. Wang, J. Wang, T. Gui, and Q. Wu, "Dual-band terahertz metamaterial absorber with polarization insensitivity and wide incident angle," *Progress In Electromagnetics Research*, Vol. 115, 381–397, 2011.

22. Yu, A., F. Yang, and A. Z. Elsherbeni, "A dual band circularly

polarized ring antenna based on composite right and left handed metamaterials," *Progress In Electromagnetics Research*, Vol. 78, 73–81, 2008.

23. Wongkasem, N., A. Akyurtlu, J. Li, A. Tibolt, Z. Kang, and W. D. Goodhue, "Novel broadband terahertz negative refractive index metamaterials: Analysis and experiment," *Progress In Electromagnetics Research*, Vol. 64, 205–218, 2006.

24. Sabah, C. and H. G. Roskos, "Dual-band polarization-independent sub-terahertz fishnet metamaterial," *Curr. Appl. Phys.*, Vol. 12, 443–450, 2012.

25. Dewar, G., "Candidates for $\mu < 0$, $\varepsilon < 0$ nanostructures," *Int. J. Mod. Phys. B*, Vol. 15, 3258–3265, 2001.

26. Vella-Coleiro, G. P., "Resonant motion of domain walls in yttrium gadolinium iron garnets," *J. Appl. Phys.*, Vol. 43, 2428–2430, 1972.

27. Tsutaoka, T., M. Ueshima, T. Tokunaga, T. Nakamura, and K. Hatakeyama, "Frequency dispersion and temperature variation of complex permeability of Ni-Zn ferrite composite materials," *J. Appl. Phys.*, Vol. 78, 3983–3991, 1995.

28. Zhao, H., J. Zhou, Q. Zhao, B. Li, L. Kang, and Y. Bai, "Magnetotunable left-handed material consisting of yttrium iron garnet slab and metallic wires," *Appl. Phys. Lett.*, Vol. 91, 131107, 2007.

29. Dewar, G., "A thin wire array and magnetic host structure with $n < 0$," *J. Appl. Phys.*, Vol. 97, 10Q101, 2005.

30. He, Y., P. He, S. D. Yoon, P. V. Parimi, F. J. Rachford, V. G. Harris, and C. Vittoria, "Tunable negative index metamaterial using yttrium iron garnet," *J. Magn. Magn. Mater.*, Vol. 313, 187–191, 2007.

31. He, P., J. Gao, Y. Chen, P. V. Parimi, C. Vittoria, and V. G. Harris, "Q-band tunable negative refractive index metamaterial using Sc-doped BaM hexaferrite," *J. Phys. D: Appl. Phys.*, Vol. 42, 155005, 2009.

32. Xu, F., Y. Bai, L. Qiao, H. Zhao, and J. Zhou, "Realization of negative permittivity of Co_2Z hexagonal ferrite and left-handed property of ferrite composite material," *J. Phys. D: Appl. Phys.*, Vol. 42, 025403, 2009.

33. Zhao, H., J. Zhou, L. Kang, and Q. Zhao, "Tunable two-dimensional left-handed material consisting of ferrite rods and metallic wires," *Opt. Express*, Vol. 17, 13373–13380, 2009.

34. Poo, Y., R.-X. Wu, G.-H. He, P. Chen, J. Xu, and R.-F. Chen,

"Experimental verification of a tunable left-handed material by bias magnetic fields," *Appl. Phys. Lett.*, Vol. 96, 161902, 2010.

35. Huang, Y. J., G. J. Wen, Y. J. Yang, and K. Xie, "Tunable dual-band ferrite-based metamaterials with dual negative refractions," *Appl. Phys. A*, Vol. 106, 79–86, 2011.

36. Smith, D. R., D. C. Vier, T. Koschny, and C. M. Soukoulis, "Electromagnetic parameter retrieval from inhomogeneous metamaterials," *Phys. Rev. E*, Vol. 71, 036617, 2005.